

# PD-1 Blockade Boosts Radiofrequency Ablation-Elicited Adaptive Immune Responses against Tumor

Liangrong Shi<sup>1,2,3</sup>, Lujun Chen<sup>1,3</sup>, Changping Wu<sup>1,2,3</sup>, Yibei Zhu<sup>4</sup>, Bin Xu<sup>1,3</sup>, Xiao Zheng<sup>1,3</sup>, Mingfen Sun<sup>1,3</sup>, Wen Wen<sup>4</sup>, Xichao Dai<sup>1,2,3</sup>, Min Yang<sup>1,2,3,4</sup>, Quansheng Lv<sup>4</sup>, Binfeng Lu<sup>5</sup>, and Jingting Jiang<sup>1,3</sup>

## Abstract

**Purpose:** Radiofrequency ablation (RFA) has been shown to elicit tumor-specific T-cell immune responses, but is not sufficient to prevent cancer progression. Here, we investigated immune-suppressive mechanisms limiting the efficacy of RFA.

**Experimental Design:** We performed a retrospective case-controlled study on patients with synchronous colorectal cancer liver metastases who had received primary tumor resection with or without preoperative RFA for liver metastases. Tumor-infiltrating T cells and tumoral PD-L1 expression in human colorectal cancer tissues were analyzed by immunohistochemistry. T-cell immune responses and PD-1/PD-L1 expression were also characterized in an RFA mouse model. In addition, the combined effect of RAF and PD-1 blockade was evaluated in the mouse RFA model.

**Results:** We found that RFA treatment of liver metastases increased not only T-cell infiltration, but also PD-L1 expression

in primary human colorectal tumors. Using mouse tumor models, we demonstrated that RFA treatment of one tumor initially enhanced a strong T-cell-mediated immune response in tumor. Nevertheless, tumor quickly overcame the immune responses by inhibiting the function of CD8<sup>+</sup> and CD4<sup>+</sup> T cells, driving a shift to higher regulatory T-cell to Teff ratio, and upregulating PD-L1/PD-1 expression. Furthermore, we established that the combined therapy of RFA and anti-PD-1 antibodies significantly enhanced T-cell immune responses, resulting in stronger antitumor immunity and prolonged survival.

**Conclusions:** The PD-L1–PD-1 axis plays a critical role in dampening RFA-induced antitumor immune responses, and this study provides a strong rationale for combining RFA and the PD-L1/PD-1 blockade in the clinical setting. *Clin Cancer Res*; 22(5); 1173–84. ©2016 AACR.

## Introduction

Radiofrequency ablation (RFA) is widely used as a local treatment for tumors such as small hepatocellular carcinomas, renal cancer, and solitary colorectal cancer liver metastases (CRCLM; refs. 1–3). RFA induces localized coagulation necrosis and leads to the release of large amounts of cellular debris *in situ*, which can serve as a source of tumor antigens to elicit host adaptive immune responses against tumors (4). Several studies on preclinical ani-

mal models have shown that localized tumor ablation by RFA can induce systemic T-cell-mediated antitumor immunity (5–7). Antigen-specific T-cell immune responses were also observed in patients with hepatic tumors after RFA therapy (8, 9). However, the RFA-induced immune responses are not sufficient to prevent tumor recurrence. The underlying mechanisms remain obscure.

Programmed death-ligand 1 (PD-L1; officially called CD274), an important immune checkpoint molecule, is often upregulated on tumor cells and tumor-associated myeloid cells. It impairs T-cell-mediated immune responses upon engagement with its cognate co-inhibitory receptor PD-1 (officially called PDCD1), which is always highly expressed on tumor-infiltrating lymphocytes (TIL; refs. 10–12). PD-L1 expression can be induced by pro-inflammatory cytokines, especially type II IFN, as an important self-limiting mechanism to prevent rampant autoimmunity (11, 13). Recent studies show that PD-L1 expression on tumor cells is associated with T-cell infiltration, suggesting that PD-L1 is actively involved in suppressing antitumor immune responses in the tumor microenvironment (TME; refs. 13–15). Whether the PD-L1–PD-1 axis is involved in modulating the antitumor T-cell immune responses induced by RFA is unclear.

The objective of this investigation was to study the RFA-induced immune responses in tumor tissues from cancer patients and tumor-bearing mice. We first examined tumor specimens from a unique cohort of colorectal cancer patients to establish whether RFA induces immune responses against tumor and potential involvement of PD-L1/PD-1 in limiting such immune responses. Mouse models were then used to characterize RFA-induced immune responses and PD-L1/PD-1-mediated immune

<sup>1</sup>Department of Tumor Biological Treatment, The Third Affiliated Hospital, Soochow University, Changzhou, Jiangsu, China. <sup>2</sup>Department of Oncology, The Third Affiliated Hospital, Soochow University, Changzhou, Jiangsu, China. <sup>3</sup>Jiangsu Engineering Research Center for Tumor Immunotherapy, Changzhou, Jiangsu, China. <sup>4</sup>Institute of Biotechnology, Key Laboratory of Clinical Immunology of Jiangsu Province, Soochow University, Jiangsu Suzhou, China. <sup>5</sup>Department of Immunology, University of Pittsburgh, Pittsburgh, Pennsylvania.

**Note:** Supplementary data for this article are available at Clinical Cancer Research Online (<http://clincancerres.aacrjournals.org/>).

L. Shi and L. Chen contributed equally to this article.

**Corresponding Authors:** Binfeng Lu, University of Pittsburgh, 200 Lothrop Street, E1047, Pittsburgh, PA 15213. Phone: 412-648-9339; Fax: 412-648-9339; E-mail: [binfeng@pitt.edu](mailto:binfeng@pitt.edu); Changping Wu, The Third Affiliated Hospital, Soochow University, Changzhou 213003, Jiangsu, China, [wcpjtt@163.com](mailto:wcpjtt@163.com); and Jingting Jiang, Department of Tumor Biological Treatment, The Third Affiliated Hospital, Soochow University, Changzhou, Jiangsu, China, [jiangjingting@suda.edu.cn](mailto:jiangjingting@suda.edu.cn)

**doi:** 10.1158/1078-0432.CCR-15-1352

©2016 American Association for Cancer Research.

### Translational Relevance

Accumulating evidence suggests that efficacy of the anti-PD-1 therapy is closely associated with pre-existing antitumor immune responses. Therefore, eliciting tumor-specific T-cell immune responses should synergize with current "checkpoint" therapies. We first demonstrated that RFA increased T-cell infiltration as well as PD-L1 expression in tumor micro-environment in a unique cohort of patients with synchronous colorectal cancer liver metastases. Using mouse tumor models, we demonstrated that the PD-L1–PD-1 axis was involved in limiting RFA-elicited T-cell immune responses. The combined therapy of RFA and PD-1 blockade synergistically enhanced T-cell-mediated immune responses and tumor rejection. Our data provide a strong rationale for combining RFA and the PD-L1/PD-1 blockade therapy in the clinical setting.

suppression. Furthermore, the combination therapy of RFA and PD-1 blockade was evaluated. Our studies are designed to provide new insight into immune-suppressive mechanisms limiting RFA efficacy and explore the potential of PD-1 blockade in combination with RFA in cancer therapy.

## Materials and Methods

### Study patients

Patient selection and study: A patient database was queried for all patients having colorectal cancer from January 2007 to December 2013 at The Third Affiliated Hospital of Soochow University. A total of 391 consecutive patients with synchronous liver metastases (LM) were initially included in this study. Among them, 38 patients who received initial hepatic RFA followed by primary tumor resection were included in the RFA group, whereas other 40 patients who received initial primary tumor resection were identified as the non-RFA group. The other 313 patients were excluded for: preoperative chemotherapy and/or radiotherapy or other types of cancer treatment (242 patients), emergency surgery for complications related to primary tumor (45 patients), and initial hepatectomy (19 patients). In addition, 7 patients who had no matched endoscopic biopsy (EB) specimen were also excluded. Paired preoperative biopsy and resected tumor (RT) specimens of all 78 patients included were collected for immunohistochemical (IHC) staining. Clinical data, including age, gender, location of primary tumor and number of LM, were obtained from the database. All RT specimens were reviewed and classified according to the 7th edition of International Union Against Cancer (UICC) TNM staging system. The study design is outlined in Supplementary Fig. S1. This study was conducted according to the principles of the Declaration of Helsinki and was approved by the Ethics Committee of Soochow University.

### RFA treatment for colorectal cancer patients with liver metastases

RFA was performed percutaneously under compound anesthesia of vein and guided by ultrasonography (US or CT). All ablations were performed using the RITA 1500 generator (RITA Medical Systems Inc.). This system consists of a 150 Watt generator and a multitined expandable electrode (StarBurst XL, RITA). The multitined expandable electrode consists of a 15-gauge insu-

lated cannula and nine individual electrode tines of 10 to 15 cm in length. It was deployed *in situ* after ultrasound or CT-guided placement of the needle electrode into the target tumor. For tumors less than 3.0 cm in diameter, the multitined expandable electrode was deployed into the center of the tumor. Each application of RFA energy lasted for 15 to 25 minutes to gain a 5.0 cm ablation zone. For tumors larger than 3.0 cm, multiple overlapping zones of ablation were needed for the destruction of the tumor and a surrounding rim of non-tumor liver. For patients with more than one lesion, the tumors were ablated separately.

### Immunohistochemistry procedures and evaluation

Formalin-fixed, paraffin-embedded tissues were processed for immunohistochemical staining with antibodies for PD-L1 (1:500, clone: SP142, Spring Bioscience), which has been used in prior clinical studies (16, 17), CD4 (clone: SP35, Maixin Biotechnology Co.), and CD8 (clone: SP16, Maixin Biotechnology Co.). The quantification of PD-L1 staining for tumor cells and lymphocytes were completed in 5% to 10% increments as previously described (14). Positive PD-L1 expression was defined as  $\geq 5\%$  cells with membranous staining. An adjusted score representing PD-L1 expression on lymphocytes was calculated as the percentage of lymphocytes stained positive for PD-L1 multiplied by the extent of lymphocytic infiltration (0 = absent, 1 = focal, 2 = moderate, and 3 marked; ref. 18). PD-L1 staining in melanoma and human placenta specimens was used as positive control (Supplementary Fig. S2). The evaluation of the number of TIL has been described previously (19). In brief, tumor-infiltrating T cells in tumor nest were counted as follows: five areas in tumor nest with the most intense T lymphocytes infiltration were selected at low magnification ( $\times 40$ ), and subsequently counted and recorded at high-power field (HPF,  $\times 200$  magnification). Results from the five areas were averaged and used in the statistical analysis.

### Cell lines and cell culture

The mouse colon cancer cell line CT26, the mouse melanoma cancer cell line B16, and the mouse breast cancer cell line 4T1 were obtained from Chinese Academy of Sciences, Shanghai Institutes for Biological Sciences.

### Animal models and treatments

A total of  $1 \times 10^6$  CT26 or B16 cells were symmetrically injected i.d. into male BALB/C and C57BL/6 mice on bilateral flanks, respectively. Treatments were initiated when the tumor volume reached about  $500 \text{ mm}^3$ . RFA was carried out only for the tumor on the right flank. RFA was performed using a 17-gauge single ablation electrode (RITA Medical Systems Inc.) with 1 cm active tip inserted percutaneously and orthogonal to the skin in the center of the tumor. Treatments were administered for 3.5 to 4.5 minutes at the target temperature of  $70^\circ\text{C}$  to ensure complete ablation of the target tumors. PD-1 blockade was accomplished by administering  $200 \mu\text{g}$  anti-PD-1 (clone: J43, BioXCell) through i.p. injection to mice every 3 days for a total of four times. To deplete  $\text{CD8}^+$  T-cell,  $250 \mu\text{g}$  anti-CD8 (clone 2.43; Bio-XCell) was delivered per mouse four times by i.p. injection every 3 days, starting from 1 day before RFA. Perpendicular diameters of the tumor on the left flanks were measured using calipers every 3 days. Tumor size was calculated using the formula  $L \times W$ , where  $L$  is the longest dimension and  $W$  is the perpendicular dimension.

### Flow cytometric analysis

The tumor lymphocytes were harvested according to the method described in our previous study (20). In brief, the tumor masses were removed, minced, and digested with collagenase and hyaluronidase solution. The cell suspension was filtered through a cell mesh and resuspended in Hank's media plus 1% FCS for further analysis. Antibodies to PD-L1 (MIH5), PD-1 (RPM1-30), CD4 (GK1.5), CD8 (53-6.7), IFN- $\gamma$  (XMG1.2), TNF- $\alpha$  (MP6-XT22), CD3 (145-2c11), Gr1 (RB6-8C5), CD11b (M1/70), CD45 (30-F11), FOXP3 (FJK-16S), eomes (Dan11mag), CD244 (eBio244F4) and CD160 (eBioALC48) were purchased from eBioscience. F4/80 (BM8), CD11c (N418), and Tim-3 (B8.2C12) antibodies were purchased from Biolegend. Flow cytometric analysis was performed using a FACS flow cytometer (Becton Dickinson). For intracellular cytokine staining, harvested cells were stimulated with PMA (10 ng/mL) and ionomycin (1  $\mu$ g/mL) for 4 h and incubated for the last 1 hour with brefeldin A (10  $\mu$ g/mL). IFN $\gamma$  and TNF $\alpha$  producing cells were examined with flow cytometry.

### ELISPOT assay

Elispot assay was performed according to the instructions of the instrument manufacturer and as described before (21). Enzyme-linked immunosorbent spot (ELISPOT) plates (MABTECH AB-plus; Sweden, Product code: 3321-4APT-4) were washed four times with sterile PBS (200  $\mu$ L/well) and incubated with medium containing 10% serum for 30 minutes at room temperature. 4T1 breast cancer cells were pulsed with 10 mg/mL of AH1 peptide (SPSYVYHQF) overnight. A total of  $10^6$  CD8<sup>+</sup> T cells isolated from spleen or draining lymph node (DLN) were plated in quadruplicates to be cocultured with pulsed or non-pulsed  $10^5$  4T1 cells. These cells were later stimulated with 1 mmol/L of phorbol 12-myristate 13-acetate and 10 ng/mL of Ionomycin as positive controls and with medium alone as negative controls. The plates were incubated in a 37°C humidified incubator with 5% CO<sub>2</sub> for 24 hours. Rat anti-mouse IFN $\gamma$  mAb (R4-6A2-biotin, 1  $\mu$ g/mL) was used for detection. After 2-hour incubation with detection antibody, the plates were washed and incubated with Streptavidin-ALP for 1 hour at room temperature. Finally, substrate solution (BCIP/NBT-plus) was added to develop spots and analysis was done using an ELISPOT Plate Reader (iSPOT, German).

### Quantitative real-time PCR

The mRNA levels of IFN $\gamma$ , TNF $\alpha$ , PD-1, PD-L1, and the reference gene  $\beta$ -actin were measured by real-time PCR machine, ABI 7500 (Applied Biosystem). In brief, total RNA was extracted from tissues, according to the manufacturer's instructions, using a total RNA purification kit (Shenergy Biocolor BioScience & Technology Company). The quality of the RNA was determined by measuring the absorbance at 260/280 nm. Using the First Strand cDNA Synthesis Kit (Fermentas), according to the manufacturer's instructions, 2  $\mu$ g total RNA was reverse transcribed to cDNA. The primers and TaqMan probes of IFN $\gamma$ , TNF $\alpha$ , PD-1, PD-L1, and the reference gene  $\beta$ -actin were designed according to the National Center for Biotechnology Information (NCBI) database by using Primer Premier 5.0 software (Palo Alto). The sequences of all primers used in this study are listed in Supplementary Table S1.

### Statistical analysis

Differences in distribution of selected demographic and clinical characteristics between RFA and non-RFA groups were performed using the Student *t* test and Fisher  $\chi^2$  test. We examined correlation

between PD-L1 expression on tumor cells and intensity of T-cell infiltration, using the pearman test. The Wilcoxon signed rank test was used to test differences in intensity of T-cell infiltration and PD-L1 expression between matched specimens (EB vs resected primary tumor) within RFA and non-RFA groups, respectively. The Mann-Whitney *U* test was used to examine differences between two groups. Logistical regression analysis was used to identify potential associated with increase of PD-L1 expression in RT specimens compared with EB specimens.

Data from animal experiments were expressed as mean  $\pm$  SEM for biologic replicates and mean  $\pm$  SD for technical replicates. The two-tailed unpaired Student *t* test was used for comparison of two groups (RFA-treated mice and control). ANOVA test was used for comparisons of groups in studies involving combinations of RFA with anti-PD-1. Survival data were analyzed by the log-rank test. A *P* value of <0.05 was considered statistically significant. Data were analyzed using SPSS software (Version 13.0, SPSS Inc.).

## Results

### Both the number of TILs and expression of PD-L1 were increased in the primary tumor upon RFA treatment of colorectal hepatic metastases

It has been shown that RFA induced systemic tumor antigen-specific T-cell responses in human carcinoma. However, there are insufficient studies on the immune modulation of TME outside of the ablation zone. To study how RFA modifies TME in human cancer patients, we performed a retrospective study of a unique cohort of patients who suffered from synchronous CRCLM. Thirty-eight patients who received preoperative RFA for LM followed by primary tumor resection were assigned to the RFA group, whereas 40 patients who received primary tumor resection without RFA were included in the non-RFA group. There was no significant difference in demographic, clinical characteristics, and staging between the RFA and non-RFA groups (Supplementary Table S2). The median time interval from RFA to primary tumor resection was 6 days (range, 4–10 days).

We first sought to determine whether RFA induces T-cell immune responses in TME using the frequency of CD4<sup>+</sup> and CD8<sup>+</sup> TIL as an indicator. There was no difference in the number of infiltrating T cells between RFA and non-RFA groups before treatment, as shown in results obtained using the EB specimens (Mann-Whitney test, *P* = 0.268 for CD8<sup>+</sup> T-cell, *P* = 0.812 for CD4<sup>+</sup> T cell, Table 1). Interestingly, however, a higher number of tumor-infiltrating T cells were observed in the RFA group compared with that of the non-RFA group in RT specimens (Mann-Whitney test, *P* < 0.001 for CD8<sup>+</sup> T cell, *P* = 0.001 for CD4<sup>+</sup> T cell, Table 1). In addition, the CD8 to CD4 ratio was higher in the RFA group compared with the non-RFA group in the RT specimens (Fisher  $\chi^2$  test, *P* = 0.002, Table 1, Fig. 1A, Supplementary Fig. S3). These data indicated that RFA elevated T-cell immune responses in TME.

We also compared the intensity of T-cell infiltration between matched EB and RT specimens on case by case basis. As shown in a previous study (22), for the non-RFA group, the number of infiltrating T cell in RT specimen was similar to that in EB specimen (Wilcoxon Signed Ranks test, *P* = 0.117 for CD8<sup>+</sup> and *P* = 0.754 for CD4<sup>+</sup>, respectively). In contrast, in the RFA group, the frequency of infiltrating CD8<sup>+</sup> and CD4<sup>+</sup> T cell was significantly increased in the RT specimens when compared with the EB

**Table 1.** Analysis of the IHC staining of CD8 and CD4 in matched EB and RT specimens

	EB		<i>P</i>	RT		<i>P</i>
	Non-RFA <i>N</i> (%)	RFA <i>n</i> (%)		Non-RFA <i>n</i> (%)	RFA <i>n</i> (%)	
CD8			0.268			<0.001
<10	12 (30.0)	10 (26.3)		14 (35.0)	2 (5.3)	
10–20	9 (22.5)	10 (26.3)		9 (22.5)	7 (18.4)	
21–40	12 (30.0)	12 (31.6)		11 (27.5)	15 (39.5)	
>40	7 (17.5)	6 (15.8)		6 (15.0)	14 (36.8)	
CD4			0.812			0.001
<10	8 (20.0)	7 (18.5)		9 (22.5)	4 (10.5)	
10–20	10 (25.0)	11 (28.9)		11 (27.5)	7 (18.5)	
21–40	13 (32.5)	10 (26.3)		12 (30.0)	14 (36.8)	
>40	9 (22.5)	10 (26.3)		8 (20.0)	13 (34.2)	
CD8:CD4 ratio			1.000			0.007
≤1	23 (57.5)	22 (52.6)		25 (62.5)	12 (34.2)	
>1	17 (42.5)	16 (47.4)		15 (37.5)	26 (65.8)	

specimens (Wilcoxon Signed Ranks test,  $P = 0.003$  and  $P = 0.002$ , respectively). In addition, in the RFA group, a higher CD8 to CD4 ratio was found in the RT specimens when compared with the EB specimens (Fisher  $\chi^2$  test,  $P = 0.002$ , Fig. 1A, Supplementary Fig. S3), consistent with the idea that a strong CD8<sup>+</sup> T-cell-mediated immune response is promoted by RFA.

We also characterized the PD-L1 expression in tumor tissues because it is an important checkpoint molecule limiting T-cell responses. PD-L1 expression was found on both tumor cells and tumor-associated immune cells. Among 78 EB specimens, 18 (23.1%; 9 each for the RFA and non-RFA groups) showed positive PD-L1 expression on tumor cells. 31 (39.7%; 14 of the RFA group and 17 of the non-RFA group) showed significant PD-L1 expression on infiltrating immune cells. Among the RT specimens, 25 (32.1%; 15 of RFA group and 10 of the non-RFA group) had PD-L1 expression on tumor cells, whereas 40 (51.3%; 22 of the RFA group and 18 of the non-RFA group) had PD-L1 expression on immune cells. In all groups, levels of PD-L1 expression on tumor cells were significantly associated with PD-L1 expression on immune cells. Both EB and RT specimens showed a significant association between PD-L1 expression on tumor cells and the intensity of CD8<sup>+</sup> T-cell infiltration (Spearman correlation,  $P = 0.001$  for EB and  $P < 0.001$  for RT specimens; Supplementary Fig. S4A and S4C). In contrast, there is no significant association between tumor PD-L1 expression and intensity of CD4<sup>+</sup> T-cell infiltration (Spearman correlation,  $P = 0.159$ , for EB and  $P = 0.065$  for RT specimens; Supplementary Fig. S4B and S4D).

We sought to determine whether RFA treatment resulted in changes of PD-L1 expression. In the non-RFA group, PD-L1 expression in the RT specimens was similar to that in the matched EB specimen (Wilcoxon signed ranks test,  $P = 0.234$  for PD-L1 expression on tumor cells and  $P = 0.194$  for that on immune cells, Fig. 1B and E). In contrast, within the RFA group, an increase of PD-L1 expression was observed not only on tumor cells but also on immune cells in the RT specimens when compared with matched EB specimens (Wilcoxon signed ranks test,  $P = 0.0001$  and  $P = 0.0003$ , respectively; Fig. 1A, C, and F; Supplementary Fig. S3). Interestingly, 78.6% of the cases that were PD-L1 positive at the initial biopsy had increases in PD-L1 expression after RFA. Moreover, 33.3% of the cases that were PD-L1 negative at the initial biopsy became PD-L1 positive for the matched RT specimens after RFA.

To more accurately demonstrate the impact of hepatic RFA on the PD-L1 expression in primary tumors, we introduced a

new variable " $\Delta$ PD-L1" ( $\Delta$ PD-L1 on tumor cell = percentage of positive cells in the RT specimen—the percentage of positive cells in the EB specimen;  $\Delta$ PD-L1 on immune cell = adjusted IHC score in the RT specimen—IHC score in the EB specimen). This variable also helps control for variations in the baselines that may affect the quantification of PD-L1 expression.  $\Delta$ PD-L1 on both tumor cells and immune cells were higher in the RFA group than in the non-RFA group (Mann-Whitney  $U$  test,  $P = 0.0004$  and  $P < 0.0001$ , respectively, Fig. 1D and G). In addition, after adjustment for other variables, including sex, year, tumor grade, histologic type, numbers of LM, the site of primary tumor, regional lymph node status, we revealed a significant association between hepatic RFA and increased PD-L1 expression in primary tumor [OR, 25.71; 95% confidence interval (CI), 4.52–146.16;  $P < 0.001$ ; Supplementary Table S3]. Collectively, this suggests that RFA of metastatic tumors induced T-cell-mediated immune responses against primary tumor as well as PD-L1 expression as a self-limiting mechanism.

#### RFA induces modest and short-lived growth inhibition of distant tumors

To further study RFA-induced immune responses, mice were inoculated with CT26, a murine colon cancer cell line that has shown sensitivity to checkpoint blockade (23), on bilateral flanks. RFA was then performed on the tumor at the right flank once the tumor volume reached about 500 mm<sup>3</sup>. The growth of the tumor at the left flank was monitored. A slight halt of growth of the contralateral tumor was observed after the RFA. However, on around days 6 to 9, the contralateral tumor restored its progressive growth (Fig. 2A). We also confirmed this finding with the B16 melanoma model (Fig. 2B).

#### Infiltrating T cells in the distant tumor displayed a potent but transient antitumor effector function, which waned as the tumor regained its growth

To better understand the magnitude and duration of antitumor immune responses induced by RFA, we performed immune analysis at an earlier and later time points in the distant CT26 tumor after RFA treatment. On day 3, about 2-fold increase of the percentage of the CD45<sup>+</sup> immune cells was observed in the distant tumor of the RFA-treated mice. Interestingly, the frequency of CD45<sup>+</sup> infiltrating cells increased further on day 8 (Supplementary Fig. S5A–S5C). This indicated that localized tumor

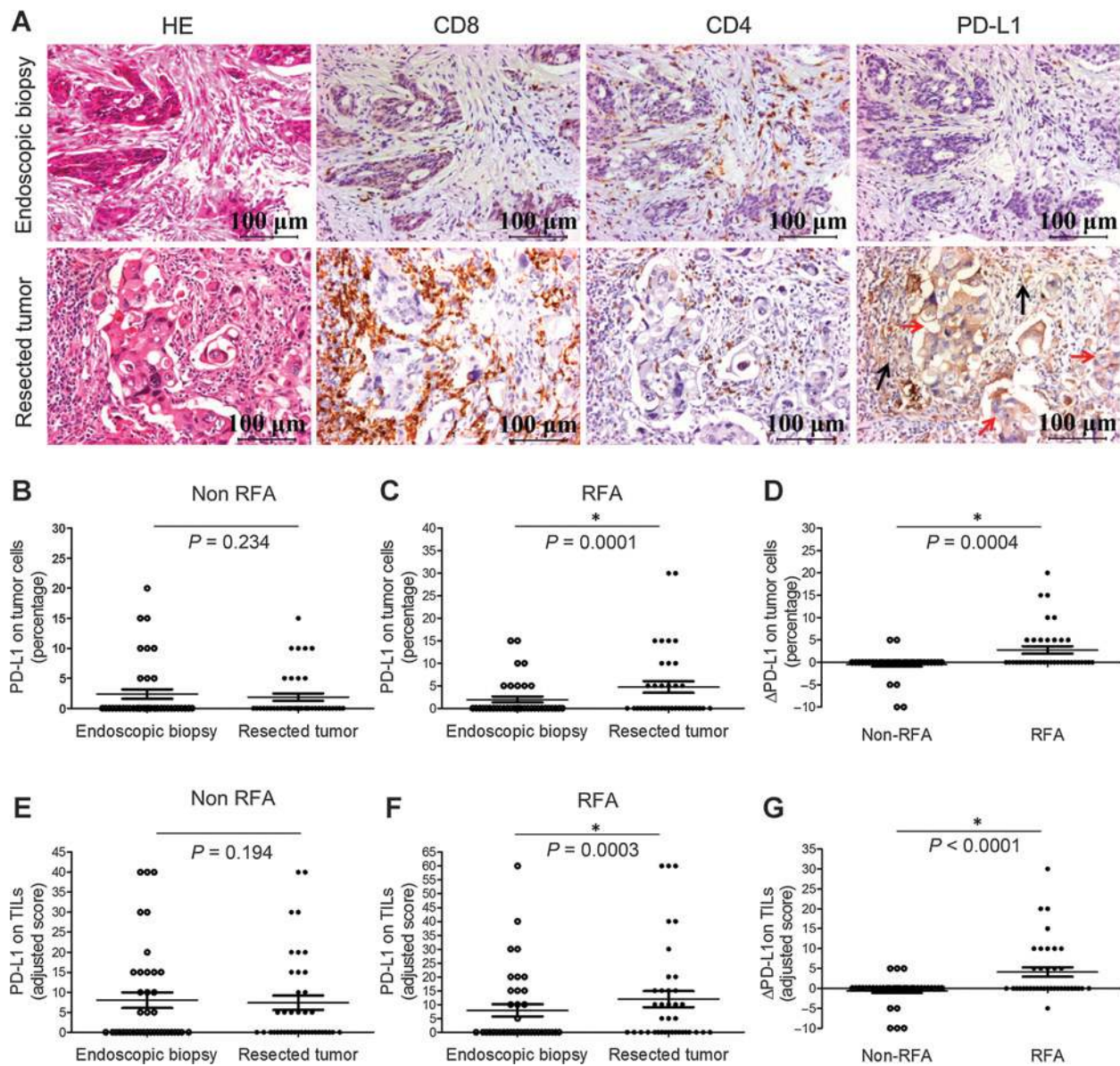


**Figure 1.** Both the number of TILs and expression of PD-L1 are increased in the primary tumor upon RFA of colorectal liver metastases. A, representative microphotographs showing hematoxylin and eosin (H&E), CD8, CD4, and PD-L1 staining of matched EB (top) and RT specimens (bottom). Top row shows CD8<sup>+</sup> and CD4<sup>+</sup> cell infiltrations and negative PD-L1 expression in EB specimen (×200); bottom row shows increased infiltration of CD8<sup>+</sup>, higher CD8 to CD4 ratio, and positive PD-L1 expression on immune cells (black arrow) and tumor cells (red arrow) in RT specimens that were obtained 9 days after hepatic RFA. B, the percentage of PD-L1 membranous expression on tumor cells in matched EB and RT specimens in the non-RFA group. C, the percentage of PD-L1 membranous expression on tumor cells in the RFA group. D, ΔPD-L1 on tumor cells (ΔPD-L1 = percentage of tumor cells expressing PD-L1 in RT specimen - percentage of tumor cells expressing PD-L1 in EB specimen) in non-RFA and RFA groups. E, adjusted score of PD-L1 expression on infiltrating immune cells in EB and RT specimens in the non-RFA group. F, adjusted score of PD-L1 expression on infiltrating immune cells in the RFA group. G, ΔPD-L1 on immune cells (ΔPD-L1 = adjusted scores in RT specimen - adjusted scores in EB specimen). The Wilcoxon signed ranks test was used in B, C, E, and F. The Mann-Whitney U test was used in D and G.

ablation induced a sustained inflammatory response in the distant tumor even at a later stage when tumor had restored rapid growth. The T-cell infiltration was characterized by increased frequencies of CD4<sup>+</sup> and CD8<sup>+</sup> T cells on days 3 and 8 (Fig. 3A-C; Supplementary Fig. S5D and S5E). The percentage of regulatory T cell (Treg) was reduced in RFA-treated mice on day 3 (Fig. 3D and E). This resulted in an increase in the ratio of CD8 versus Treg (Fig. 3F), indicating a shift of immune balance toward

antitumor immunity on day 3 upon RFA. However, the shift was temporary. On day 8, the percentage of Treg was at a similar level to that in the untreated mice (Fig. 3D and E). On day 8 after RFA, the CD8<sup>+</sup> T cell to Treg ratio was significantly decreased as comparing with that on day 3 ( $P < 0.001$ ), whereas it was still modestly higher due to an increase in CD8<sup>+</sup> T-cell infiltration (Fig. 3F). Similar results were obtained using the B16 melanoma tumor model (Supplementary Fig. S6A-S6G). These results suggest that

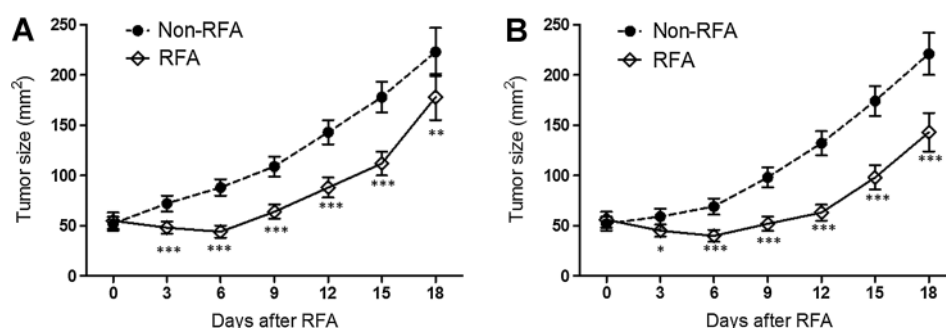


**Figure 2.**

RFA induces slight and short-lived inhibition of distant tumor. A total of  $1 \times 10^6$  CT26 or B16 cells were injected i.d. into male BALB/C and C57BL/6 mice, respectively, on bilateral flanks symmetrically. RFA was administered for the right tumor when the tumor volume reached about  $500 \text{ mm}^3$ . The size of the left tumor was measured every three days after RFA. A, representative data from the CT26 model. B, representative data from the B16 model. Ten mice were included in each group; error bars, SEM; \*,  $P < 0.05$ ; \*\*,  $P < 0.01$ ; \*\*\*,  $P < 0.001$ .

an antitumor immune response is induced by RFA, but is tamed by the active immune suppression in TME.

To determine the function of TIL, we analyzed the ability of T cells to produce  $\text{IFN}\gamma$  and  $\text{TNF}\alpha$  by flow cytometry. On day 3, the percentage of  $\text{IFN}\gamma^+$  and  $\text{TNF}\alpha^+$   $\text{CD8}^+$  TIL was significantly increased in RFA-treated mice when compared with untreated mice. However, the percentage of  $\text{IFN}\gamma^+$  and  $\text{TNF}\alpha^+$   $\text{CD8}^+$  TIL was markedly decreased on day 8 and was similar to that in the untreated mice (Fig. 3G and H). Similar results were observed on  $\text{CD4}^+$  TIL (Fig. 3G and I). In addition,  $\text{IFN}\gamma$  and  $\text{TNF}\alpha$  mRNA expression in tumors were 4- to 5-fold higher in RFA-treated mice compared with untreated mice on day 3 (Fig. 3J and K). In contrast,  $\text{IFN}\gamma$  and  $\text{TNF}\alpha$  mRNA levels were sharply decreased on day 8 (Fig. 3J and K). These data indicate that TIL underwent functional exhaustion at the later stage after RFA when tumor regression was reversed.

#### Expression of PD-L1 and PD-1 in the distant tumor upon RFA treatment

Our data showed that both the number of TIL and expression of PD-L1 were increased in the human primary tumor upon RFA of colorectal hepatic metastases. Here, we sought to examine PD-L1 expression in the TME in CT26 mouse colon cancer model. On day 3, a rapid upregulation of PD-L1 expression was observed on  $\text{CD45}^-$  cells isolated from tumor tissues. The proportion of  $\text{PD-L1}^+ \text{CD45}^-$  cells increased from about 10% to 23% (Fig. 4A and B). Similarly, PD-L1 expression increased in tumor associated DCs, MDSCs, and macrophages upon RFA (Fig. 4A and B). On day 8, we observed a further increase of PD-L1 expression on all cell populations in the RFA group (Fig. 4A and C). In contrast, we did not detect PD-L1 expression on splenic  $\text{CD11c}^+$ ,  $\text{F4/80}^+$ , and  $\text{CD11b}^+ \text{Gr1}^+$  cells (Supplementary Fig. S7A). In addition, we showed that RFA treatment also led to an increase in PD-L1 expression in B16 tumor tissues (Supplementary Fig. S6H–S6J). These data indicate that the tumor inflammatory microenvironment induced by RFA plays a direct role in the upregulation of PD-L1 expression.

Further analysis showed that approximately 70% of  $\text{CD8}^+$  and 40% of  $\text{CD4}^+$  TIL expressed PD-1 in untreated CT26 tumor-bearing mice. On day 3 after RFA, we observed about a 20% decrease in  $\text{PD-1}^+ \text{CD8}^+$  TIL cells compared with those in the untreated mice. However, the frequency of  $\text{PD-1}^+ \text{CD8}^+$  TIL increased to more than 80% on day 8 in RFA-treated mice and

was slightly higher than those in the untreated mice (Fig. 4D and E). The PD-1 expression on  $\text{CD4}^+$  T cells, however, showed no difference between two groups on both days 3 and 8 (Fig. 4F). We did not detect large numbers of  $\text{PD-1}^+$  splenic  $\text{CD4}^+$  and  $\text{CD8}^+$  T cells on both days 3 and 8 (Supplementary Fig. S7B and S7C). In B16 tumor, we detected a slight but statistically significant increase of PD-1 expression on both  $\text{CD4}^+$  and  $\text{CD8}^+$  TIL on day 8 after RFA (Supplementary Fig. S6K–S6N).

Our data also showed a significant increase in PD-L1 mRNA in  $\text{CD45}^-$  cells and total tumors on both days 3 and 8 in CT26 tumor (Fig. 4G). The mRNA level of PD-1 in total tumor had no significant change on day 3 after RFA, but increased 3-fold on day 8 (Fig. 4H). In accordance with PD-1 protein expression on  $\text{CD8}^+$  TIL, PD-1 mRNA also decreased significantly on day 3, and then increased on day 8 in the  $\text{CD8}^+$  TIL population in the RFA group compared with the non-RFA group (Fig. 4H). Collectively, these data suggest that the PD-L1/PD-1 axis is involved in limiting the efficacy of RFA treatment through immune suppression.

In addition, we found that Tim-3, CD160, CD244, and eomes, which are typical exhaustion markers (24), were expressed at higher levels on both  $\text{CD8}^+$  and  $\text{CD4}^+$  TIL 8 days after RFA treatment (Supplementary Fig. S8A–S8F). In contrast, only CD160 and CD244 were expressed at higher levels on day 3 in the RFA group compared with the control. Therefore, in addition to the PD-L1/PD-1 axis, other markers of T-cell exhaustion were also induced to higher levels upon RFA treatment.

#### The combination of RFA and anti-PD-1 treatment synergistically inhibited the growth of the distant tumor through $\text{CD8}^+$ T cells

It has been demonstrated that the efficacy of the PD-1 blockade therapy is closely associated with pre-existing tumor antigen-specific T-cell immune responses (16, 25). Because RFA induced T-cell accumulation and upregulated PD-L1 expression in distant tumor tissues, we postulated that subsequent anti-PD-1 therapy would generate a stronger antitumor immunity and improve the treatment efficacy of RFA. To test the hypothesis, CT26-bearing mice were treated with RFA plus an isotype control antibody, RFA plus anti-PD-1 monoclonal antibodies (mAbs; RFA+ $\alpha$ -PD-1), anti-PD-1 mAbs alone ( $\alpha$ -PD-1), or left without treatment (Fig. 5A). Because  $\text{CD8}^+$  TIL were significantly increased in tumors after RFA treatment, we also sought to determine whether  $\text{CD8}^+$  T cells

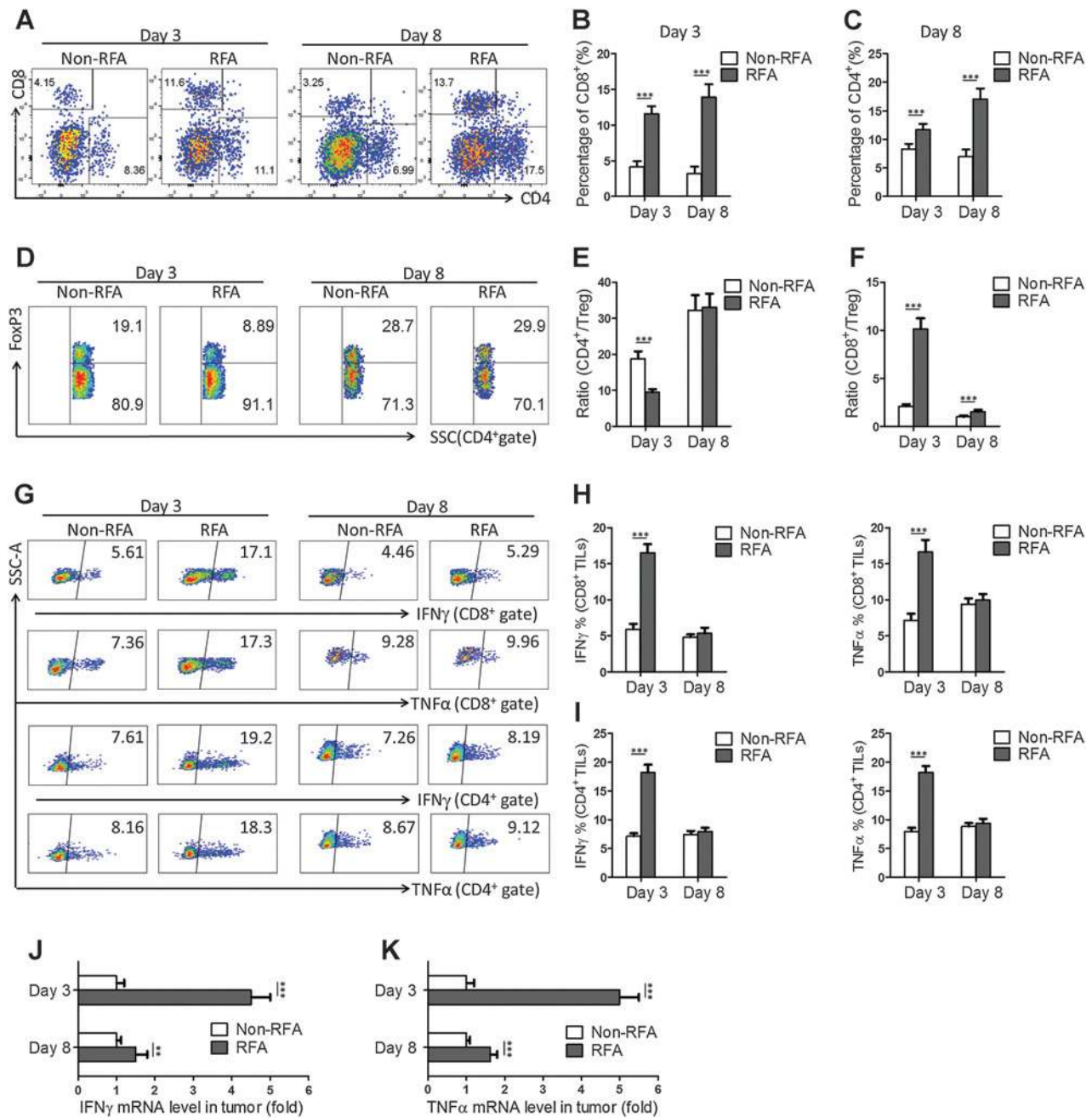


**Figure 3.** Induction of T-cell infiltration into distant tumor after RFA and analysis of the cells' functional status. A total of  $1 \times 10^6$  CT26 cells were injected i.d. into male BALB/C mice on bilateral flanks symmetrically. RFA was administrated as described in Fig. 2. On days 3 and 8 after RFA treatment, the tumors on the left flank were resected and either digested to generate single-cell suspension or used for RNA isolation. A, representative flow cytometric plots showing CD8<sup>+</sup> and CD4<sup>+</sup> cells in single-cell suspension on days 3 and 8 after RFA. B, the percentage of CD8<sup>+</sup>TIL on days 3 and 8. C, the percentage of CD4<sup>+</sup> T cells on days 3 and 8. D, flow cytometric plots showing CD4<sup>+</sup>FoxP3<sup>+</sup>Treg. E, percentages of FoxP3<sup>+</sup> within CD4<sup>+</sup> TIL. F, CD8<sup>+</sup> to Treg ratio. G, representative flow cytometric plots showing IFN $\gamma$  and TNF $\alpha$  expression on CD8<sup>+</sup> and CD4<sup>+</sup>TIL. H, percentages of IFN $\gamma$ <sup>+</sup> and TNF $\alpha$ <sup>+</sup> within CD8<sup>+</sup>TIL. I, percentages of IFN $\gamma$ <sup>+</sup> and TNF $\alpha$ <sup>+</sup> within CD4<sup>+</sup>TIL. J, the IFN $\gamma$  mRNA level in total tumor tissue analyzed by RT-QPCR on days 3 and 8. K, the TNF $\alpha$  mRNA level in total tumor tissue. Each data point represents cumulative results from two independent experiments with 5 mice per group (values represent means  $\pm$  SEM; \*\*,  $P < 0.01$ ; \*\*\*,  $P < 0.001$ ).

mediate the effect of RFA and PD-1 blockade using CD8-depleting mAbs. No recurrence occurred in the ablation zone. RFA had a modest inhibitory effect on contralateral tumor progression. Anti-PD-1 itself also led to a modest inhibition of tumor growth, consistent with a previous observation (23). In contrast, we

observed significant tumor regression, much longer duration of inhibition of tumor growth and prolonged survival in the RFA/anti-PD-1-treated mice, as compared with mice in the no-treatment or single treatment groups (Fig. 5B and C). Depletion of CD8<sup>+</sup> T cells completely eliminated the inhibition of tumor

growth of mice with the combined treatment (Fig. 5B and C). These data indicate that RFA and PD-1 blockade further enhance CD8<sup>+</sup> T-cell-mediated antitumor immunity.

**Combination of RFA and anti-PD-1 mAbs administration further enhanced tumor antigen-specific T-cell responses and increased Teff to Treg ratio in the distant tumor**

To better determine synergistic antitumor immune responses of the combination of RFA and anti-PD-1, we examined the T-cell response in mice treated with RFA,  $\alpha$ -PD-1, RFA +  $\alpha$ -PD-1, and no treatment. On day 12, the frequency of both CD45<sup>+</sup> and CD8<sup>+</sup> cells was higher in RFA-treated and  $\alpha$ -PD-1 mAbs-treated mice than in untreated mice (Fig. 5D–F, Supplementary Fig. S9A and S9B). In the RFA plus  $\alpha$ -PD-1 mAbs group, the infiltrating CD45<sup>+</sup> and CD8<sup>+</sup> cells were increased as compared with the RFA or  $\alpha$ -PD-1 alone (Fig. 5D–F, Supplementary Fig. S9A and S9B). Importantly, the percentage of IFN $\gamma$ <sup>+</sup> and TNF $\alpha$ <sup>+</sup> CD8<sup>+</sup>TIL in the RFA plus  $\alpha$ -PD-1 mAbs-treated mice increased 3-fold more than the RFA-treated mice and 2-fold more than  $\alpha$ -PD-1 mAbs-treated mice (Fig. 5G and H). Meanwhile, the number of CD4<sup>+</sup> TIL and the percentage of IFN $\gamma$ <sup>+</sup> and TNF $\alpha$ <sup>+</sup> CD4<sup>+</sup>TIL were increased in mice receiving combined therapy (Fig. 5G, I, and Supplementary Fig. S9C). Quantitative real-time PCR analysis showed that mRNA levels of IFN $\gamma$  and TNF $\alpha$  in contralateral tumor were significantly elevated in the RFA plus  $\alpha$ -PD-1-treated mice when compared with the RFA or the  $\alpha$ -PD-1 treatment alone groups (Fig. 5J). These data suggest that blockade of the PD-L1–PD-1 pathway boosted

RFA-induced antitumor immune responses and reversed immune suppression at the distant tumor site.

To explore whether systemic tumor antigen-specific T cells can be induced to a higher level after the combined treatment, we carried out ELISPOT assays for IFN $\gamma$  secretion upon *ex vivo* restimulation of T cells with tumor antigens. CD8<sup>+</sup> T cells isolated from spleens and DLNs were co-cultured with AH1 peptide pulsed with antigen-presenting cells (APC). Consistent with the increased number of CD8<sup>+</sup> T cells producing IFN $\gamma$  in tumor, we detected a significant increase in the number of tumor antigen-specific IFN $\gamma$ -secreting cells in both spleens and DLNs from the RFA/ $\alpha$ -PD-1-treated mice compared with the RFA or the  $\alpha$ -PD-1 treatment alone groups (Fig. 5K). Thus, these data indicated that RFA and anti-PD-1 therapy synergistically induced adaptive tumor antigen-specific CD8<sup>+</sup> T-cell immune responses.

The PD-L1–PD-1 pathway has been shown to be required for the abundance of Treg in the tumor sites. To assess the impact of PD-1 blockade on the balance between intratumoral Teff and Treg, we examined CD4<sup>+</sup>FoxP3<sup>+</sup>Treg in contralateral tumor on day 12 after RFA. Our data showed that the proportion of intratumoral Treg was significantly decreased both in mice treated with RFA/anti-PD-1 and anti-PD-1 alone, leading to dramatically elevated CD8<sup>+</sup> T cell to Treg ratio as compared with the RFA-treated mice or anti-PD-1-treated mice (Fig. 5L–N). Collectively, these data suggest anti-PD-1 therapy reverses adaptive immunosuppression in the distant tumor through reducing Treg and increasing functional effector T cells.

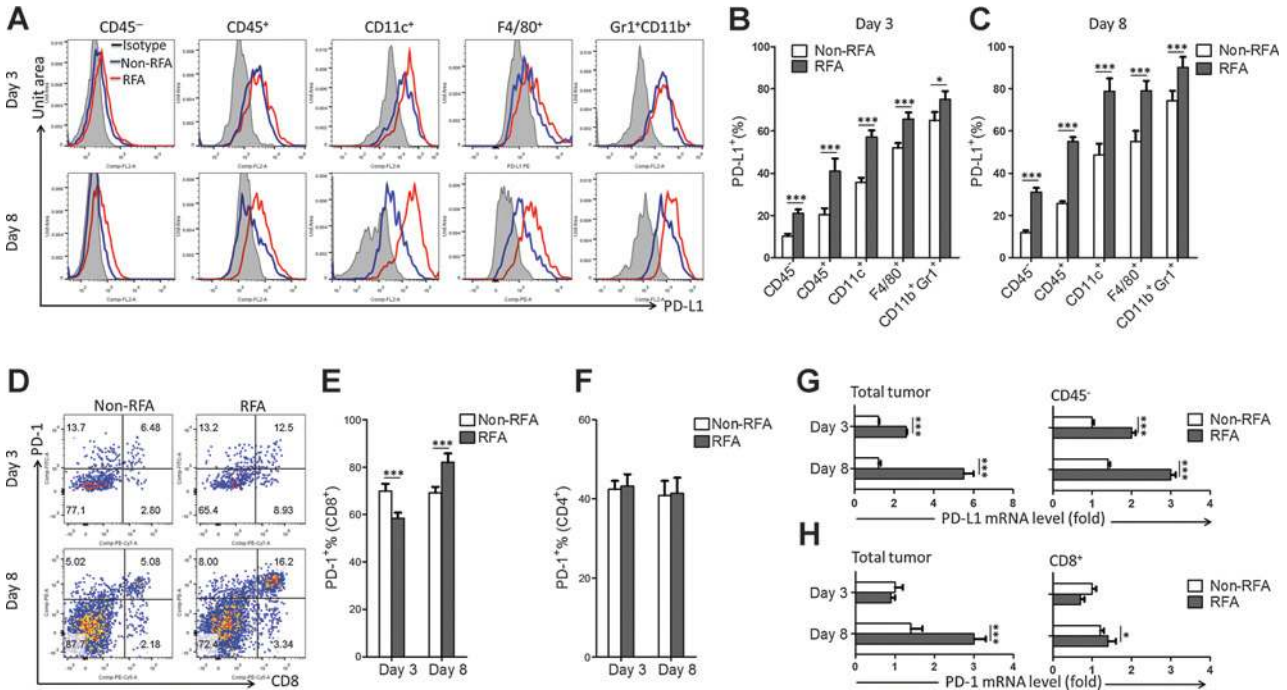


**Figure 4.** PD-L1/PD-1 expression in the distant tumor after RFA treatment in the CT26 tumor-bearing mice. The CT26 tumor-bearing mice models were established and treated as described in Fig. 3. A, representative flow cytometric histograms showing PD-L1 expression on tumor and stromal cells (CD45<sup>-</sup>), total infiltrating immune cells (CD45<sup>+</sup>), dendritic cells (CD11c<sup>+</sup>), macrophages (F4/80<sup>+</sup>), and MDSCs (Gr1<sup>+</sup>CD11b<sup>+</sup>) in contralateral tumor on days 3 and 8 after RFA. B, percentages of PD-L1<sup>+</sup> cells on day 3 upon RFA. C, percentages of PD-L1<sup>+</sup> cells on day 8. D, representative flow cytometric plots showing PD-1 expression on CD8<sup>+</sup> cells within CD45<sup>+</sup> population on days 3 and 8. E, percentages of PD-1<sup>+</sup> cells within CD8<sup>+</sup>TIL. F, percentage of PD-1<sup>+</sup> cells within CD4<sup>+</sup> cells. G, the PD-L1 mRNA level in total tumor (left) and isolated CD45<sup>-</sup> cells (right). H, the PD-1 mRNA level in total tumor (left) and isolated CD8<sup>+</sup>TIL (right). Data represent cumulative results from two independent experiments with 5 mice per group (values represent means  $\pm$  SEM; \*,  $P < 0.05$ ; \*\*\*,  $P < 0.001$ ).



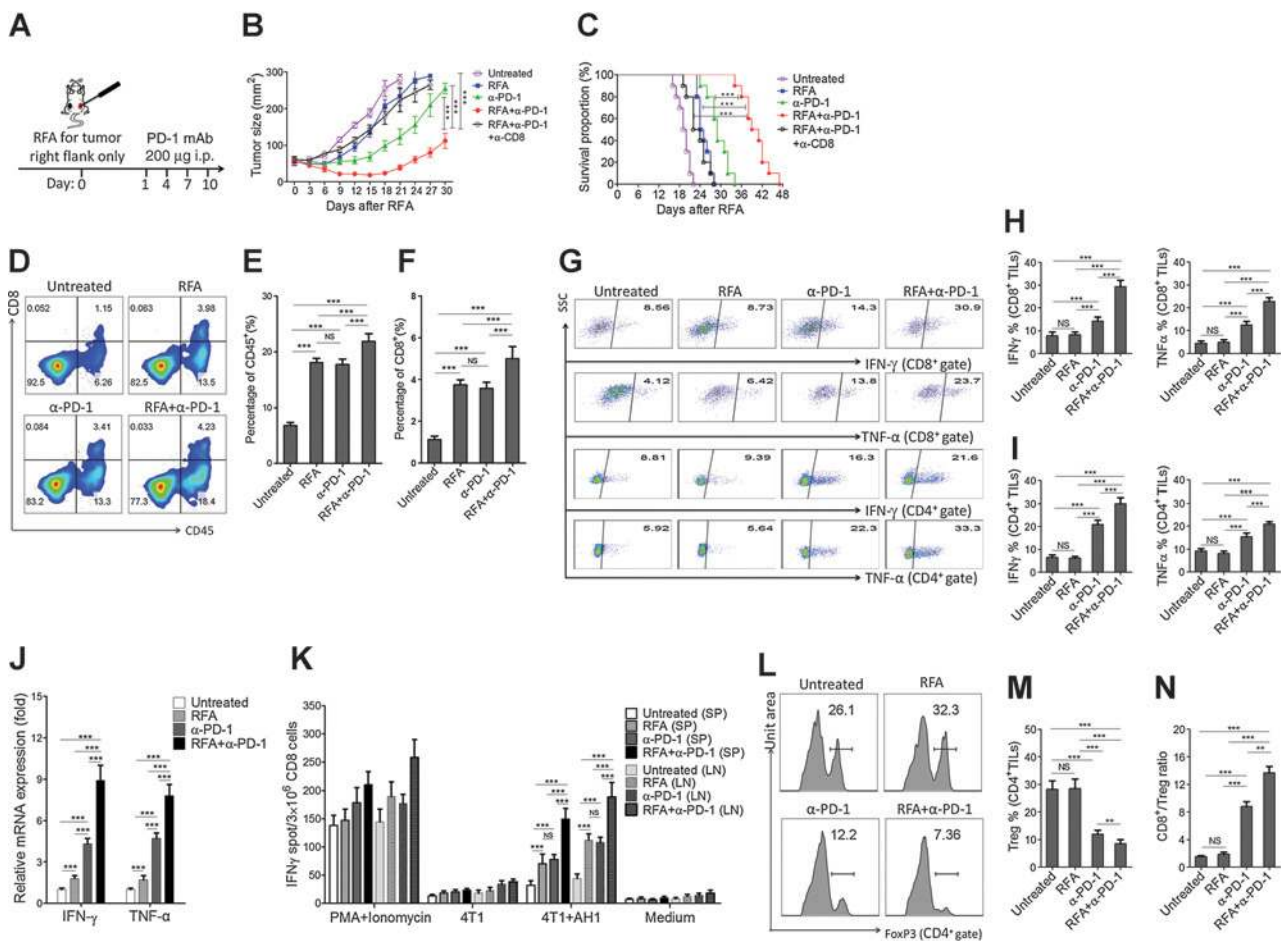


**Figure 5.** RFA and the anti-PD-1 therapy synergistically enhanced T-cell-mediated antitumor immunity. A, schematic drawing of the study. The CT26 tumor-bearing mice models were established and treated with RFA as described in Fig. 2. Anti-PD-1 mAbs were administered i.p. to mice on day 1 after RFA, and subsequently once every 3 days for a total of four times. The tumors on the left flank were resected and either digested to generate single-cell suspension or used for RNA isolation on day 12. For depletion of CD8<sup>+</sup> T cells, 250  $\mu$ g CD8 mAbs were injected i.p. starting from 1 day before RFA and subsequently once every 3 days for a total of four times. B, the size of the tumors on the left flank was monitored every 3 days after RFA (10 mice in each group). C, Kaplan-Meier survival curves are shown, and the log-rank test was performed. D, representative flow cytometric plots showing CD8<sup>+</sup> and CD45<sup>+</sup> cells in single-cell suspension on day 12 after RFA. E, percentages of CD45<sup>+</sup> cells within single-cell suspension. F, percentages of CD8<sup>+</sup>TIL. G, representative flow cytometric plots of IFN $\gamma$ - and TNF $\alpha$ -expressing CD8<sup>+</sup> and CD4<sup>+</sup>TIL. H, percentages of IFN $\gamma$ <sup>+</sup> and TNF $\alpha$ <sup>+</sup> within CD8<sup>+</sup>TIL. I, percentages of IFN $\gamma$ <sup>+</sup> and TNF $\alpha$ <sup>+</sup> within CD4<sup>+</sup>TIL. J, the mRNA level of IFN $\gamma$  and TNF $\alpha$  in tumor tissues analyzed by RT-QPCR. K, detection of IFN $\gamma$  secretion by CD8<sup>+</sup>T cells in the spleens (SP) and DLNs (LN) in response to AHI peptide by ELISPOT. L, representative flow cytometric histogram showing CD4<sup>+</sup> FoxP3<sup>+</sup> Treg. M, percentages of FoxP3<sup>+</sup> within CD4<sup>+</sup> TIL. N, CD8<sup>+</sup> to Treg ratio. Data represent results from one of two independent experiments with 5 mice per group (values represent means  $\pm$  SEM; \*\*,  $P < 0.01$ ; \*\*\*,  $P < 0.001$ ).

Besides PD-1, multiple pathways have been found to be involved in TIL exhaustion (24). In particular, we and others have found that Tim-3 was highly induced in CD4<sup>+</sup> and CD8<sup>+</sup> TIL in both mouse and human tumors (26–28). Interestingly, we observed a significant increase of Tim-3 on both CD8<sup>+</sup> and CD4<sup>+</sup> TIL upon PD-1 blockade, RFA treatment, or combination treatment (Supplementary Fig. S10A–S10D). These data suggest that additional regulatory pathways such as Tim-3 might compensate for the lack of PD-1 to induce TIL exhaustion.

## Discussion

In this study, we have shown that localized RFA increases T-cell infiltration as well as PD-L1 expression in a distant tumor in both human patients with synchronous colorectal cancer liver metastases and tumor-bearing mice. Furthermore, using a mouse

model, we demonstrated that combination of localized RFA and anti-PD-1 antibodies significantly enhanced tumor antigen-specific T-cell responses, increased intratumoral Teff to Treg ratio, and synergistically inhibited growth of the distant tumor.

It has been shown that RFA induced systemic tumor antigen-specific T-cell immune responses in human hepatocellular carcinoma (8, 9). However, these studies are limited to the analysis of peripheral immune cells but not in TME. Because of extensive application of RFA in CRCLM (2) and promotion of "liver first" treatment modality (initial liver resection/ablation followed by primary tumor resection) in resectable synchronous CRCLM (29), we could obtain matched tumor specimens outside of the ablation zone (primary colorectal tumors) prior-RFA (EB) and post-RFA (RT). Using this novel clinical study design, we revealed a significant increase in T-cell infiltration and a higher CD8 to CD4 ratio in the primary colorectal tumor tissues after RFA for liver

metastases. These data clearly demonstrated that the localized RFA induced T-cell-mediated immune responses in a distant tumor site in human carcinoma. However, RFA is not sufficient to prevent tumor recurrence in clinic, suggesting that duration and function of RFA-induced tumor-specific T cells are inadequate. In this study, we showed that local RFA led to a small and short-lived inhibition of distant tumors in mouse models. We further showed that frequency of IFN $\gamma$  and TNF $\alpha$ -producing CD8<sup>+</sup> TIL increased at the early stage after RFA but diminished overtime. In addition, we found that the PD-L1–PD-1 axis plays an important role in mediating suppression of RFA-induced antitumor immunity. Besides PD-L1 and PD-1, CTLA-4 has been shown to inhibit thermal ablation–induced antitumor activities (4, 30, 31). Aside from immune inhibitory pathways, it has been shown that various cytokines that are used to enhance T-cell homeostasis and T-cell immune responses also increase the antitumor efficacy of RFA (32, 33). Thus, future combination therapy with RFA and various immune modulators can be explored in the clinical setting.

The abscopal effect we observed with RFA has been described in other tumor therapies. Notably, radiotherapy has been recently shown to induce similar antitumor effect through induction of tumor antigen–specific adaptive immune responses (34, 35). Blockade of immune checkpoints has been shown to improve the efficacy of radiotherapy on local and distant tumors in experimental systems and as well as in clinical settings (36–38). In a recent report, Victor and colleagues (39) showed a phase I clinical trial of 22 patients with advanced melanoma treated with radiotherapy and anti–CTLA-4. They also found radiotherapy combined with anti–CTLA-4 enhanced antitumor immunity, but did not prevent T-cell exhaustion in the melanoma tumor mouse model. Similar to our study, PD-L1 blockade reversed T-cell exhaustion, promoted T-cell expansion, mitigate depression in the CD8/Treg ratio, and led to an optimal response in their preclinical model. Despite similarity between RFA and radiotherapy in the final outcome of induction of adaptive immunity against tumor antigens, the underlying mechanisms could differ. A recent study showed that STING but not MyD88 or TRIF is essential for radiotherapy and the cGAS–STING axis mediates innate sensing of irradiated-tumor cells (40). It remains elusive what triggers innate immunity and set off adaptive immunity in the setting of RFA and the underlying mechanism warrants further studies.

Blockade of the PD-L1–PD-1 axis has achieved remarkable efficacy in clinical trials (17, 41–45). Nevertheless, most patients who lack PD-L1 expression do not benefit from the anti–PD-1 therapy (42), suggesting that efficacy of the anti–PD-1 therapy is closely associated with pre-existing antitumor immune responses (16, 25, 46). Thus, rational combination of treatments that can induce antitumor immune responses and the anti–PD-L1/PD-1 therapy should greatly increase the number of suitable cancer patients. Recently, combining of radiotherapy and PD-L1/PD-1 blockade have been shown to synergistically enhance antitumor immunity in preclinical studies (36, 47, 48), suggesting local antitumor treatments, which can elicit immune response hold promise in providing opportunity for PD-1/PD-L1 blockade therapy.

## References

1. Duan C, Liu M, Zhang Z, Ma K, Bie P. Radiofrequency ablation versus hepatic resection for the treatment of early-stage hepatocellular carcinoma

Taube and colleagues (46) have shown that the PD-L1 expression in colorectal cancer was relatively lower in contrast with other cancer types such as melanoma, kidney cancer, and lung cancer etc. In this study, we also revealed a low frequency of PD-L1 expression. Interestingly, we demonstrated that RFA for liver metastases upregulated PD-L1 expression, which is associated with an increase in T-cell infiltration in primary colorectal cancer. On one hand, these findings indicate that RFA-stimulated antitumor immune responses are dampened by PD-L1. On the other hand, our studies strongly suggest that RFA increases the number of patients that can potentially benefit from the powerful anti–PD-L1–PD-1 therapy.

There are several potential advantages of combining RFA and the PD-L1/PD-1 blockade. First, RFA is widely used in CRC LM (49), making it feasible to explore its role in a novel combined modality. Second, RFA results in the instant release of large amounts of tumor antigens in the milieu of "danger" signals, which can potentially stimulate transient immune responses to a wide of variety of tumor antigens. Third, the PD-1 mAbs treatment has shown promising results in colorectal cancer in a phase I clinical trial (45), and a study showed that the microsatellite instable subset of colorectal cancer can be a good candidate for checkpoint blockade immunotherapy (50). Thus, these results and our study strongly support combining RFA and blockade of the PD-L1/PD-1 for the treatment of metastatic colorectal cancer patients.

## Disclosure of Potential Conflicts of Interest

No potential conflicts of interest were disclosed.

## Authors' Contributions

**Conception and design:** L. Shi, C. Wu, Y. Zhu, B. Lu, J. Jiang  
**Development of methodology:** L. Chen, C. Wu, Y. Zhu, B. Lu  
**Acquisition of data (provided animals, acquired and managed patients, provided facilities, etc.):** L. Shi, L. Chen, C. Wu, M. Sun, W. Wen, X. Dai, M. Yang, Q. Lv, B. Lu  
**Analysis and interpretation of data (e.g., statistical analysis, biostatistics, computational analysis):** C. Wu, B. Xu, B. Lu  
**Writing, review, and/or revision of the manuscript:** L. Shi, L. Chen, C. Wu, X. Zheng, X. Dai, B. Lu, J. Jiang  
**Administrative, technical, or material support (i.e., reporting or organizing data, constructing databases):** L. Shi, C. Wu, Y. Zhu, B. Lu  
**Study supervision:** C. Wu, B. Lu

## Acknowledgments

This work was supported by grants from the National Natural Science Foundation of China (nos. 30972703, 81171653, 81201741, 31428005, 31570877, 31570908, and 81301960). The project was also supported by the NIH through grants (no. R21CA167229, UL1 RR024153, UL1TR000005, and IP50 CA097190), Roswell Park Cancer Institute/University of Pittsburgh Cancer Institute Ovarian Cancer Specialized Programs of Research Excellence Grants (P50CA159981), and the Key R&D Projects of Science and Technology Department of Jiangsu Province (BE2015633 and BE2015634).

The costs of publication of this article were defrayed in part by the payment of page charges. This article must therefore be hereby marked *advertisement* in accordance with 18 U.S.C. Section 1734 solely to indicate this fact.

Received June 9, 2015; revised September 4, 2015; accepted September 25, 2015; published online March 1, 2016.

meeting Milan criteria: a systematic review and meta-analysis. *World J Surg Oncol* 2013;11:190.

2. Solbiati L, Ahmed M, Cova L, Ierace T, Brioschi M, Goldberg SN. Small liver colorectal metastases treated with percutaneous radiofrequency ablation: local response rate and long-term survival with up to 10-year follow-up. *Radiology* 2012;265:958–68.
3. Popovic P, Lukic S, Mijailovic M, Salapura V, Garbajs M, Surlan Popovic K. Percutaneous radiofrequency ablation of small renal cell carcinoma: technique, complications, and outcomes. *J BUON* 2012;17:621–6.
4. den Brok MH, Suttmuller RP, van der Voort R, Bennink EJ, Figdor CG, Ruers TJ, et al. In situ tumor ablation creates an antigen source for the generation of antitumor immunity. *Cancer Res* 2004;64:4024–9.
5. Wissniewski TT, Hansler J, Neureiter D, Frieser M, Schaber S, Esslinger B, et al. Activation of tumor-specific T lymphocytes by radio-frequency ablation of the VX2 hepatoma in rabbits. *Cancer Res* 2003;63:6496–500.
6. Dromi SA, Walsh MP, Herby S, Traugher B, Xie J, Sharma KV, et al. Radiofrequency ablation induces antigen-presenting cell infiltration and amplification of weak tumor-induced immunity. *Radiology* 2009;251:58–66.
7. Lin WX, Fifs T, Malcontenti-Wilson C, Nikfarjam M, Muralidharan V, Nguyen L, et al. Induction of Th1 immune responses following laser ablation in a murine model of colorectal liver metastases. *J Transl Med* 2011;9:83.
8. Mizukoshi E, Yamashita T, Arai K, Sunagazaka H, Ueda T, Arihara F, et al. Enhancement of tumor-associated antigen-specific T-cell responses by radiofrequency ablation of hepatocellular carcinoma. *Hepatology* 2013;57:1448–57.
9. Nobuoka D, Motomura Y, Shirakawa H, Yoshikawa T, Kuronuma T, Takahashi M, et al. Radiofrequency ablation for hepatocellular carcinoma induces glypican-3 peptide-specific cytotoxic T lymphocytes. *Int J Oncol* 2012;40:63–70.
10. Dong H, Zhu G, Tamada K, Chen L. B7-H1, a third member of the B7 family, co-stimulates T-cell proliferation and interleukin-10 secretion. *Nat Med* 1999;5:1365–9.
11. Zou W, Chen L. Inhibitory B7-family molecules in the tumour microenvironment. *Nat Rev Immunol* 2008;8:467–77.
12. Dong H, Strome SE, Salomao DR, Tamura H, Hirano F, Flies DB, et al. Tumor-associated B7-H1 promotes T-cell apoptosis: a potential mechanism of immune evasion. *Nat Med* 2002;8:793–800.
13. Spranger S, Spaepen RM, Zha Y, Williams J, Meng Y, Ha TT, et al. Up-regulation of PD-L1, IDO, and TIGIT in the melanoma tumor microenvironment is driven by CD8(+) T cells. *Sci Transl Med* 2013;5:200ra116.
14. Taube JM, Anders RA, Young GD, Xu H, Sharma R, McMiller TL, et al. Colocalization of inflammatory response with B7-h1 expression in human melanocytic lesions supports an adaptive resistance mechanism of immune escape. *Sci Transl Med* 2012;4:127ra37.
15. McCray AJ, Hallett R, Bernard D, Swift SL, Zhu Z, Teoderascu F, et al. Immunotherapy-induced CD8<sup>+</sup> T cells instigate immune suppression in the tumor. *Mol Ther* 2014;22:206–18.
16. Herbst RS, Soria JC, Kowanetz M, Fine GD, Hamid O, Gordon MS, et al. Predictive correlates of response to the anti-PD-L1 antibody MPDL3280A in cancer patients. *Nature* 2014;515:563–7.
17. Powles T, Eder JP, Fine GD, Braith F, Loriot Y, Cruz C, et al. MPDL3280A (anti-PD-L1) treatment leads to clinical activity in metastatic bladder cancer. *Nature* 2014;515:558–62.
18. Thompson RH, Gillett MD, Chevillat JC, Lohse CM, Dong H, Webster WS, et al. Costimulatory B7-H1 in renal cell carcinoma patients: indicator of tumor aggressiveness and potential therapeutic target. *Proc Natl Acad Sci U S A* 2004;101:17174–9.
19. Jing S, Lujun C, Guangbo Z, Jingting J, Ming Z, Yan T, et al. Clinical significance and regulation of the costimulatory molecule B7-H3 in human colorectal carcinoma. *Cancer Immunol Immunother* 2010;59:1163–71.
20. Zhu Y, Ju S, Chen E, Dai S, Li C, Morel P, et al. T-bet and oesodermin are required for T cell-mediated antitumor immune responses. *J Immunol* 2010;185:3174–83.
21. Davis MB, Vasquez-Dunndel D, Fu J, Albesiano E, Pardoll D, Kim YJ. Intratumoral administration of TLR4 agonist absorbed into a cellular vector improves antitumor responses. *Clin Cancer Res* 2011;17:3984–92.
22. Koelzer VH, Lugli A, Dawson H, Hadrich M, Berger MD, Borner M, et al. CD8/CD45RO T-cell infiltration in endoscopic biopsies of colorectal cancer predicts nodal metastasis and survival. *J Transl Med* 2014;12:81.
23. Selby MJ, Engelhardt JJ, Quigley M, Henning KA, Chen T, Srinivasan M, et al. Anti-CTLA-4 antibodies of IgG2a isotype enhance antitumor activity through reduction of intratumoral regulatory T cells. *Cancer Immunol Res* 2013;1:32–42.
24. Wherry EJ, Kurachi M. Molecular and cellular insights into T-cell exhaustion. *Nat Rev Immunol* 2015;15:486–99.
25. Tumei PC, Harview CL, Yearley JH, Shintaku IP, Taylor EJ, Robert L, et al. PD-1 blockade induces responses by inhibiting adaptive immune resistance. *Nature* 2014;515:568–71.
26. Fourcade J, Sun Z, Benallaoua M, Guillaume P, Luescher IF, Sander C, et al. Upregulation of Tim-3 and PD-1 expression is associated with tumor antigen-specific CD8<sup>+</sup> T-cell dysfunction in melanoma patients. *J Exp Med* 2010;207:2175–86.
27. Gao X, Zhu Y, Li G, Huang H, Zhang G, Wang F, et al. TIM-3 expression characterizes regulatory T cells in tumor tissues and is associated with lung cancer progression. *PLoS ONE* 2012;7:e30676.
28. Sakuishi K, Apetoh L, Sullivan JM, Blazar BR, Kuchroo VK, Anderson AC. Targeting Tim-3 and PD-1 pathways to reverse T-cell exhaustion and restore anti-tumor immunity. *J Exp Med* 2010;207:2187–94.
29. de Jong MC, van Dam RM, Maas M, Bemelmans MH, Olde Damink SW, Beets GL, et al. The liver-first approach for synchronous colorectal liver metastasis: a 5-year single-centre experience. *HPB* 2011;13:745–52.
30. den Brok MH, Suttmuller RP, Nierkens S, Bennink EJ, Frielink C, Toonen LW, et al. Efficient loading of dendritic cells following cryo and radiofrequency ablation in combination with immune modulation induces anti-tumour immunity. *Br J Cancer* 2006;95:896–905.
31. Waitz R, Solomon SB, Petre EN, Trumble AE, Fasso M, Norton L, et al. Potent induction of tumor immunity by combining tumor cryoablation with anti-CTLA-4 therapy. *Cancer Res* 2012;72:430–9.
32. Johnson EE, Yamane BH, Buhtoiarov IN, Lum HD, Rakhmilevich AL, Mahvi DM, et al. Radiofrequency ablation combined with KS-IL2 immunocytokine (EMD 273066) results in an enhanced antitumor effect against murine colon adenocarcinoma. *Clin Cancer Res* 2009;15:4875–84.
33. Iida N, Nakamoto Y, Baba T, Nakagawa H, Mizukoshi E, Naito M, et al. Antitumor effect after radiofrequency ablation of murine hepatoma is augmented by an active variant of CC Chemokine ligand 3/macrophage inflammatory protein-1alpha. *Cancer Res* 2010;70:6556–65.
34. Apetoh L, Ghiringhelli F, Tesniere A, Obeid M, Ortiz C, Criollo A, et al. Toll-like receptor 4-dependent contribution of the immune system to anticancer chemotherapy and radiotherapy. *Nat Med* 2007;13:1050–9.
35. Lee Y, Auh SL, Wang Y, Burnette B, Meng Y, Beckett M, et al. Therapeutic effects of ablative radiation on local tumor require CD8<sup>+</sup> T cells: changing strategies for cancer treatment. *Blood* 2009;114:589–95.
36. Deng L, Liang H, Burnette B, Beckett M, Darga T, Weichselbaum RR, et al. Irradiation and anti-PD-L1 treatment synergistically promote antitumor immunity in mice. *J Clin Invest* 2014;124:687–95.
37. Postow MA, Callahan MK, Barker CA, Yamada Y, Yuan J, Kitano S, et al. Immunologic correlates of the abscopal effect in a patient with melanoma. *N Engl J Med* 2012;366:925–31.
38. Verbrugge J, Hagekyriakou J, Sharp LL, Galli M, West A, McLaughlin NM, et al. Radiotherapy increases the permissiveness of established mammary tumors to rejection by immunomodulatory antibodies. *Cancer Res* 2012;72:3163–74.
39. Twyman-Saint Victor C, Rech AJ, Maity A, Rengan R, Pauken KE, Stelekati E, et al. Radiation and dual checkpoint blockade activate non-redundant immune mechanisms in cancer. *Nature* 2015;520:373–7.
40. Deng L, Liang H, Xu M, Yang X, Burnette B, Arina A, et al. STING-dependent cytosolic DNA sensing promotes radiation-induced type I interferon-dependent antitumor immunity in immunogenic tumors. *Immunity* 2014;41:843–52.
41. Hamid O, Robert C, Daud A, Hodi FS, Hwu WJ, Kefford R, et al. Safety and tumor responses with lambrolizumab (anti-PD-1) in melanoma. *N Engl J Med* 2013;369:134–44.
42. Topalian SL, Hodi FS, Brahmer JR, Gettinger SN, Smith DC, McDermott DF, et al. Safety, activity, and immune correlates of anti-PD-1 antibody in cancer. *N Engl J Med* 2012;366:2443–54.
43. Ribas A. Tumor immunotherapy directed at PD-1. *N Engl J Med* 2012;366:2517–9.
44. Topalian SL, Sznol M, McDermott DF, Kluger HM, Carvajal RD, Sharfman WH, et al. Survival, durable tumor remission, and long-term safety in patients with advanced melanoma receiving nivolumab. *J Clin Oncol* 2014;32:1020–30.

45. Lipson EJ, Sharfman WH, Drake CG, Wollner I, Taube JM, Anders RA, et al. Durable cancer regression off-treatment and effective reinduction therapy with an anti-PD-1 antibody. *Clin Cancer Res* 2013;19:462–8.
46. Taube JM, Klein A, Brahmer JR, Xu H, Pan X, Kim JH, et al. Association of PD-1, PD-1 ligands, and other features of the tumor immune microenvironment with response to anti-PD-1 therapy. *Clin Cancer Res* 2014;20:5064–74.
47. Dovedi SJ, Adlard AL, Lipowska-Bhalla G, McKenna C, Jones S, Cheadle EJ, et al. Acquired resistance to fractionated radiotherapy can be overcome by concurrent PD-L1 blockade. *Cancer Res* 2014;74:5458–68.
48. Victor CT, Rech AJ, Maity A, Rengan R, Pauken KE, Stelekati E, et al. Radiation and dual checkpoint blockade activate non-redundant immune mechanisms in cancer. *Nature* 2015;520:373–7.
49. Wong SL, Mangu PB, Choti MA, Crocenzi TS, Dodd GD III, Dorfman GS, et al. American Society of Clinical Oncology 2009 clinical evidence review on radiofrequency ablation of hepatic metastases from colorectal cancer. *J Clin Oncol* 2010;28:493–508.
50. Xiao Y, Freeman GJ. The microsatellite instable subset of colorectal cancer is a particularly good candidate for checkpoint blockade immunotherapy. *Cancer Discov* 2015;5:16–8.